Available online at www.sciencedirect.com
ScienceDirect
Lithos 99 (2007) 68–84
LITHOS
www.elsevier.com/locate/lithos

Amphiboles from suprasubduction and intraplate lithospheric mantle

Massimo Coltorti [a,*], Costanza Bonadiman [a], Barbara Faccini [a], Michel Grégoire [b], Suzanne Y. O'Reilly [c], William Powell [c]

[a] Department of Earth Sciences, Ferrara University Polo Scientifico-Tecnologico, Blocco B, Via Saragat 1 - 44100 FERRARA, Italy
[b] CNRS Observatoire Midi-Pyrénées, 14 Av. E. Belin, 31400 Toulouse, France
[c] ARC National Key Centre for Geochemical Evolution and Metallogeny of Continents (GEMOC) Department of Earth & Planetary Sciences Macquarie University NSW 2109, Australia

Received 25 May 2006; accepted 15 May 2007
Available online 12 June 2007

Abstract

Geochemical features of amphiboles, mainly from mantle xenoliths, were investigated for a number of intraplate and suprasubduction localities, with the aim of fingerprinting the metasomatic signatures for the two different geological settings. Amphiboles generated in the mantle wedge above subduction zones (suprasubduction amphibole, S-Amph) are depleted in Nb, with suprachondritic Ti/Nb and Zr/Nb ratios, whereas intraplate amphibole (I-Amph) is enriched in Nb, with subchondritic Ti/Nb and Zr/Nb ratios. These complementary features can be reconciled by Nb-depleted fluids coming off the subducted oceanic crust, leaving a rutile-bearing eclogite residuum. Rutile is a major repository for High Field Strength Elements (mainly Nb, Ta and Ti), with a preference to retain pentavalent elements. During the subduction process, rutile-bearing eclogite will continue its descent into the lower part of the upper mantle (or even below), generating a subchondritic Ti/Nb or Zr/Nb reservoir. The partial incorporation of this material in an asthenospheric plume will ultimately contribute to the genesis of intraplate alkaline basalts, characterized by high Nb contents. The link between the complementary geochemical features of suprasubduction and intraplate amphiboles suggests a relationship between calc-alkaline and intraplate magmatisms. This is also in agreement with the temporal sequence of subduction, calc-alkaline volcanism and intraplate magmatism that can be observed in several localities around the Mediterranean areas and in most subduction zones worldwide.

Keywords: Mantle metasomatism; Intraplate mantle xenoliths; Suprasubduction mantle xenoliths; Mantle HFSE; Subducted slab recycling

1. Introduction

Mantle metasomatism in anorogenic settings has been widely investigated in the last decades (e.g. Menzies et al., 1987; Siena et al., 1991; O'Reilly et al., 1991; O'Reilly and Griffin, 1996; Ionov et al., 1996, 1997; Neumann and Wulff-Pedersen, 1997; Coltorti et al., 1999; Witt-Eickschen et al., 2003; Szabo et al., 2004). Processes and nature of melts/fluids responsible for mantle metasomatism have been mostly constrained using geochemical characteristics of clinopyroxene and glass, which are the main repositories for trace elements in anhydrous mantle peridotites. Amphibole, when present, represents another important trace element acceptor and can provide additional constraints (Ionov and Hofman, 1995; Ionov et al., 1997; Powell et al., 2004; Coltorti et al., 2004). Mantle xenoliths are much rarer in calc-alkaline type magmas from orogenic environments compared with their common occurrence in highly alkaline, SiO_2-

* Corresponding author. Tel.: +39 0532 974721; fax: +39 0532 974767.
E-mail address: clt@unife.it (M. Coltorti).

0024-4937/$ - see front matter © 2007 Elsevier B.V. All rights reserved.
doi:10.1016/j.lithos.2007.05.009

undersaturated magmas from intraplate settings. Consequently, the nature and processes of fluid metasomatism in suprasubduction zones are still far from being clearly understood (Ishimaru et al., 2006 and reference therein). In addition, the inventory of trace elements such as Rb, Ba and Nb (Ta) which are not easily hosted in clinopyroxene, is a critical parameters in interpreting such phenomena in orogenic mantle domains. Although amphibole composition cannot be equated to the composition of the metasomatizing agents, amphiboles represent an ideal tool for unravelling the nature of melts and fluids migrating in the mantle wedge above subduction zones and for comparing the geochemical signatures of these melts/fluids with those from intraplate settings.

This study compares geochemical signatures of amphiboles in mantle xenoliths from both intraplate and subduction settings, in order to characterize melts and other fluids recorded by mantle metasomatic events in the

Table 1
Major and trace element analyses (average and standard deviation) of amphiboles used for defining the I-Amph field

Locality	Antarctica		Australia		West Eifel		Kerguelen	
	Mean	Standard deviation	Mean	Standard deviation	Mean	Standard deviation	Mean	Standard deviation
No. of samples	12		22		44		43	
SiO_2	42.14	0.80	44.11	1.14	43.57	1.18	42.37	0.53
TiO_2	4.31	0.56	1.22	0.95	1.78	1.24	2.57	0.91
Al_2O_3	13.62	0.32	13.45	1.40	13.45	0.83	12.30	0.31
FeO_{tot}	4.63	0.81	3.73	0.49	4.99	1.59	5.69	0.30
MnO	0.04	0.03	0.05	0.02	0.04	0.04	0.05	0.02
MgO	16.61	0.56	17.73	0.53	17.30	1.26	16.79	0.31
CaO	11.33	0.26	10.90	0.41	10.95	0.34	11.41	0.14
Na_2O	2.98	0.14	3.70	0.25	3.01	0.26	3.21	0.06
K_2O	0.95	0.14	0.71	0.34	1.35	0.29	1.11	0.04
NiO	0.04	0.05	0.10	0.02	0.08	0.07	0.09	0.05
Cr_2O_3	0.75	0.47	1.49	0.48	1.30	0.80	1.03	0.47
No. of samples	12		21		37		43	
Rb	6.75	2.51	7.27	9.19	11.1	6.41	10.9	4.23
Ba	281	38.6	231	162.2	249	128	165	79.3
Th	0.54	0.18	1.54	1.25	2.36	1.75	5.05	0.83
U	0.19	0.10	0.34	0.34	0.44	0.31	0.81	1.33
Nb	73.8	18.8	51.5	36.6	97.9	69.7	79.4	41.4
Ta	3.79	0.80	2.10	1.80	4.57	3.53	4.80	4.21
La	13.6	3.19	15.1	7.66	21.8	11.1	42.7	6.28
Ce	48.3	12.5	38.0	21.6	59.1	24.2	109	14.2
Pr	7.41	1.80	4.29	2.54	7.59	2.67		
Sr	656	141	382	239	457	126	447	82.4
Nd	35.4	7.35	22.7	14.6	30.9	11.3	46.8	6.38
Zr	124	49.2	92.0	64.2	132	123	182	102
Hf	3.90	1.55	1.78	1.73	3.20	3.20	4.33	3.22
Sm	9.44	2.04	5.16	3.25	8.84	18.8	9.24	7.28
Eu	3.14	0.63	1.66	0.89	1.69	0.54	2.72	0.39
Gd	8.59	1.86	4.81	2.35	4.83	1.45	6.23	1.01
Tb	1.14	0.22			0.70	0.20		
Dy	6.25	1.28	4.23	1.41	3.55	0.89	4.88	0.83
Y	29.7	5.09	20.4	6.64	15.4	4.20	23.6	3.50
Ho	1.10	0.17	0.73	0.21	0.62	0.13	0.94	0.15
Er	2.75	0.48	2.07	0.70	1.62	0.41	2.34	0.38
Tm	0.33	0.04			0.20	0.05		
Yb	2.09	0.44	1.80	0.72	1.24	0.30	2.26	0.31
Lu	0.26	0.04	0.24	0.11	0.16	0.05	0.31	0.06
Ti/Zr	208		79.6		80.8		84.9	
Ti/Nb	350		142		109		194	
Zr/Nb	1.68		1.79		1.35		2.29	

Data from O'Reilly et al. (1991), Yaxley and Kamenetsky (1999), Moine et al. (2001), Witt-Eickschen et al. (2003), Coltorti et al. (2004), and Powell et al. (2004).

two environments. It also contributes to the long standing debate on the origin of High Field Strength Elements (HFSE) depletion in calc-alkaline magmas and to recycling models for slab subduction in the upper mantle.

2. Data source

All studied amphiboles vary in composition between pargasite, edenite and kaersutite, the latter being exclusively present in anorogenic settings. Due to the large variety of textural occurrences no distinction has been made between incipient growing, disseminated (amph-D), veinlet or vein amphiboles (amph-V). All amphiboles from suprasubduction settings and the great majority of amphiboles from intraplate settings grow around and at the expense of cpx. Thus they appear texturally and geochemically unrelated to the host basalts. When amphibole is present as veins, in some cases, it has been interpreted as the fractionation product of a magma whose composition could be similar to the host magma, but

Table 2
Major and trace element analyses (average and standard deviation) of amphiboles used for defining the S-Amph field

Locality	Kamchatka		Lihir	Finero		Val d'Ultimo	
	Mean	Standard deviation		Mean	Standard deviation	Mean	Standard deviation
No. of samples	30		1	4		32	
SiO_2	47.69	2.69	47.80	46.51	0.96	46.15	1.10
TiO_2	0.36	0.53	0.19	0.39	0.09	0.28	0.09
Al_2O_3	10.39	1.99	8.20	10.50	0.34	11.52	0.84
FeO_{tot}	3.96	2.20	2.98	3.31	0.19	3.30	0.74
MnO	0.06	0.03	0.02	0.06	0.02	0.07	0.04
MgO	19.58	1.77	20.77	19.58	0.28	19.23	0.67
CaO	11.76	0.46	11.76	12.51	0.23	12.76	0.66
Na_2O	2.09	0.40	2.38	2.06	0.13	1.87	0.27
K_2O	0.22	0.08	0.61	0.67	0.26	0.56	0.22
NiO	0.11	0.04	0.11				
Cr_2O_3	1.07	0.80	1.86	1.90	0.29	1.13	0.22
No. of samples	17		1	4		20	
Rb	0.82	0.41	1.23	6.50	1.73	8.78	6.76
Ba	51.3	66.2	5.14	69.3	20.7	281	245
Th	0.18	0.12	1.09			1.09	0.51
U	0.08	0.04	0.14			0.49	0.25
Nb	0.56	0.60	1.37	3.35	0.72	2.98	1.80
Ta	0.10	0.06	0.07			0.15	0.10
La	1.97	2.04	19.9	17.2	3.03	8.49	4.20
Ce	6.98	7.24	42.7	33.5	7.33	18.9	10.0
Pr	1.08	1.01				2.28	1.21
Sr	83.4	51.9	840	291	15.3	102	52.5
Nd	4.88	4.09	16.4	16.6	3.51	9.18	4.87
Zr	30.8	31.7	81.2	67.0	5.10	12.0	6.91
Hf	0.97	0.97	1.70			0.46	0.33
Sm	1.25	0.82	2.82	3.78	1.00	1.65	0.88
Eu	0.55	0.48	1.06	0.87	0.21	0.51	0.19
Gd	1.12	0.93	2.08	2.55	0.76	1.67	0.74
Tb	0.22	0.14				0.25	0.10
Dy	1.16	0.98	1.87	1.48	0.40	1.61	0.76
Y	6.75	5.16	12.3	6.60	2.25	9.53	3.22
Ho	0.26	0.21	0.40			0.37	0.13
Er	0.72	0.54	1.32	0.68	0.19	1.13	0.38
Tm	0.11	0.07				0.17	0.06
Yb	0.89	0.50	1.48	0.67	0.13	1.26	0.41
Lu	0.14	0.07	0.22			0.20	0.06
Ti/Zr	69.3		14.0	34.4		138	
Ti/Nb	3799		831	689		558	
Zr/Nb	54.8		59.3	20.0		4.03	

Data from Zanetti et al. (1999), Gregoire et al. (2001), Marocchi (2006), Ishimaru et al. (2006), and Ishimaru and Arai (in press).

Table 3
Major and trace element analyses of amphiboles from Ichinomegata (Japan)

Sample	I908				I873				I883					ING1789				
Spot	am1–1	am3–1	am4–1	am5–1	am1–1	am3–1	am4–1	am4–2	am1–1	am1–2	am2–1	am3–1	am4–1	am1–1	am2–1	am3–1	am4–1	am5–1
SiO_2	43.09	42.83	42.87	42.69	42.24	42.87	42.98	42.45	42.71	42.83	42.89	42.28	42.52	43.08	45.43	44.56	45.05	44.65
TiO_2	0.87	1.25	0.71	0.48	1.33	1.18	1.16	1.22	1.28	1.26	1.25	1.04	0.88	0.82	0.63	0.68	0.54	0.60
Al_2O_3	15.38	15.09	16.39	16.58	13.77	13.58	13.13	13.80	14.59	14.58	14.53	14.92	14.93	12.64	10.91	12.02	11.05	11.22
FeO_{tot}	3.69	3.61	3.61	3.69	5.63	5.63	5.67	5.72	4.67	4.65	4.77	4.77	4.77	4.13	4.07	4.40	4.43	4.45
MnO	0.08	0.05	0.02	0.07	0.04	0.04	0.06	0.08	0.05	0.05	0.07	0.04	0.10	0.05	0.07	0.04	0.05	0.05
MgO	17.98	17.62	17.64	17.76	17.21	17.34	17.45	17.20	17.72	17.65	17.62	17.70	17.68	17.87	18.98	18.43	18.85	18.70
CaO	11.99	11.88	11.70	11.83	11.64	11.60	11.60	11.68	11.84	11.87	11.75	11.93	11.90	11.70	11.61	11.60	11.56	11.59
Na_2O	3.58	3.53	3.56	3.54	2.32	2.37	2.31	2.32	2.33	2.40	2.37	2.24	2.27	2.09	2.17	2.25	2.31	2.25
K_2O	0.01	0.00	0.02	0.01	0.93	0.84	0.83	0.97	0.98	0.85	0.82	1.19	1.12	1.06	0.69	0.70	0.46	0.45
NiO	0.11	0.17	0.08	0.08	0.12	0.10	0.11	0.15	0.11	0.15	0.12	0.12	0.10	0.14	0.08	0.10	0.12	0.13
Cr_2O_3	0.92	1.13	0.75	0.42	1.26	1.25	1.33	1.29	0.91	1.11	1.07	1.07	0.73	1.64	1.54	1.57	1.64	1.65
Total	97.69	97.16	97.34	97.15	96.49	96.78	96.63	96.88	97.19	97.38	97.27	97.29	97.00	95.22	96.17	96.35	96.07	95.74
mg#	89.67	89.68	89.69	89.55	84.48	84.57	84.56	84.27	87.10	87.11	86.81	86.87	86.83	88.51	89.25	88.17	88.33	88.21
Rb	0.11	0.15	0.11	0.18	2.91	2.94	2.00	1.85	3.98	4.54	5.22	4.31	4.22	4.67	1.89	11.0	2.76	1.65
Ba	0.26	0.63	0.87	3.25	73.7	60.7	43.1	48.4	158	109	118	136	140	73.4	40.9	219	47.6	33.1
Th	0.002	0.005	0.002	0.003	0.10	0.04	0.02	0.04	0.08	0.11	0.12	0.06	0.04	0.12	0.10	0.38	0.16	0.27
U	n.d.	0.002	0.001	0.003	0.02	n.d.	0.01	0.01	0.01	0.02	0.02	0.01	0.01	0.03	0.01	0.02	0.01	0.02
Nb	0.05	0.07	0.05	0.06	2.65	2.52	1.59	2.61	1.03	0.69	0.73	0.90	0.81	3.07	5.41	10.4	10.3	11.5
Ta	0.001	0.004	0.002	0.003	0.09	0.08	0.07	0.08	0.04	0.02	0.03	0.04	0.04	0.11	0.17	0.72	0.53	0.79
La	0.25	0.26	0.25	0.26	1.88	1.89	1.28	1.60	2.24	2.11	2.12	1.82	1.80	3.45	3.61	5.79	4.42	5.48
Ce	2.37	2.46	2.30	2.52	5.96	6.30	4.44	5.68	6.93	5.99	5.73	6.17	6.44	12.1	13.4	19.6	17.4	19.0
Pr	0.65	0.69	0.60	0.67	1.17	0.99	0.90	1.06	1.21	1.02	1.00	1.12	1.19	1.78	2.08	3.16	2.85	3.26
Sr	10.8	11.7	9.65	10.3	199	188	133	178	236	195	194	221	227	209	216	250	217	232
Nd	4.45	4.65	4.15	4.56	6.14	4.80	4.72	5.43	7.15	5.84	5.62	6.33	6.87	7.89	8.88	14.7	13.6	16.1
Zr	13.7	16.4	11.6	13.3	17.3	13.7	11.9	14.4	21.78	19.37	20.72	12.17	11.58	37.2	36.6	60.8	56.4	71.5
Hf	0.45	0.63	0.41	0.50	0.57	0.50	0.46	0.48	0.74	0.54	0.62	0.38	0.42	1.16	0.99	1.88	1.38	2.16
Sm	1.97	2.15	1.81	1.96	1.91	1.63	1.51	1.67	2.52	2.15	2.07	1.98	2.26	2.05	2.19	3.83	3.46	4.26
Eu	0.91	0.91	0.83	0.94	0.79	0.68	0.61	0.74	0.94	0.85	0.83	0.82	0.87	0.75	0.81	1.17	1.02	1.19
Gd	3.03	3.12	2.61	2.97	2.58	2.33	2.01	2.14	3.11	2.78	2.72	2.40	2.48	2.07	2.11	3.62	3.19	4.10
Tb	0.56	0.59	0.51	0.57	0.48	0.46	0.35	0.41	0.51	0.50	0.48	0.38	0.39	0.33	0.36	0.57	0.52	0.65
Dy	4.08	4.36	3.70	4.06	3.43	3.40	2.35	2.88	3.59	3.33	3.34	2.45	2.47	2.14	2.2	3.49	3.27	4.26
Y	24.4	26.9	22.5	24.8	19.9	20.5	14.0	17.2	19.4	19.9	19.7	14.1	14.3	11.8	12.6	19.5	19.1	24.8
Ho	0.92	1.01	0.87	0.93	0.79	0.80	0.53	0.63	0.74	0.75	0.74	0.54	0.54	0.47	0.48	0.74	0.70	0.92
Er	2.63	2.90	2.38	2.62	2.15	2.22	1.58	1.79	1.97	1.99	2.05	1.49	1.49	1.20	1.28	1.91	1.92	2.56
Tm	0.38	0.42	0.35	0.38	0.28	0.32	0.21	0.25	0.28	0.30	0.30	0.21	0.21	0.15	0.19	0.27	0.29	0.37
Yb	2.51	2.84	2.47	2.52	1.81	2.00	1.37	1.66	1.66	2.03	2.01	1.47	1.38	1.17	1.24	1.74	2.05	2.63
Lu	0.35	0.39	0.34	0.34	0.26	0.28	0.18	0.25	0.25	0.28	0.28	0.21	0.21	0.16	0.16	0.24	0.31	0.37

For the analytical conditions see Powell et al. (2004) and the analytical methods section of the GEMOC website (http://www.es.mq.edu.au/gemoc/). mg#=[Mg/(Mg+Fe_t)*100], n.d., not detected.

never as the result of an infiltration from the host basalt. This is more evident in those minerals analyzed in the alpine complexes.

All investigated xenoliths are spinel-bearing peridotites and garnet has not been observed. No HFSE-bearing accessory phases such as rutile, ilmenite or zircon were found. Armalcolite is reported from a few mantle xenoliths from Kerguelen (Gregoire et al., 2000), but it is clearly secondary with respect to the peridotite minerals (including amphibole) and it cannot have affected the composition of previously formed amphibole.

In order to screen the origin of the studied mantle xenoliths, the "suprasubduction" group is confined exclusively to mantle xenoliths brought to the surface by magmas with a clear calc-alkaline (sensu lato) affinity, and to two well-studied and clearly identified subduction-related peridotite bodies. This material will thus be considered representative of the lithologies of the mantle wedge above a subduction zone. On the contrary xenoliths brought to the surface by alkaline intraplate magmatism will be considered as representative of anorogenic mantle lithologies.

The data refer to well-studied localities and were chosen on the basis of trace element analyses availability. Major and trace element analyses of intraplate amphibole (I-Amph) represent a large range of continental and oceanic settings, including Eifel (Witt-Eickschen et al., 2003 and reference therein), Kerguelen (Moine et al., 2001), Antarctica (Coltorti et al., 2004), Australia

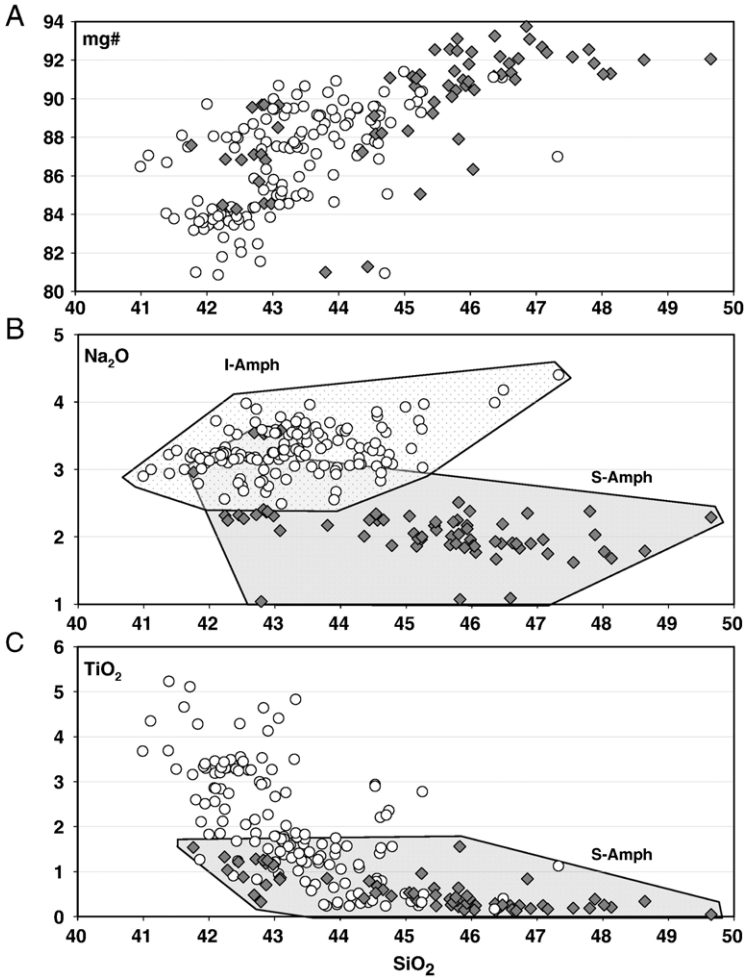

Fig. 1. mg# (A), Na_2O (B) and TiO_2 (C) vs SiO_2 diagrams for intraplate (I-Amph; open circles) and suprasubduction (S-Amph, grey diamonds) amphiboles. mg#=[Mg/(Mg+Fe_t)*100]. I-Amph field includes data from Eifel (Witt-Eickschen et al., 2003), Kerguelen (Moine et al., 2001), Antarctica (Coltorti et al., 2004), Australia (O'Reilly et al., 1991; Yaxley and Kamenetsky, 1999; Powell et al., 2004; Coltorti, unpublished data), Pannonian Basin (Bali et al., 2002), Ahaggar (Dautria et al., 1987). S-Amph field includes data from Japan (Johnson et al., 1996; Abe et al., 1998; this work), Papua New Guinea (Gregoire et al., 2001), Finero (Zanetti et al., 1999), Val d'Ultimo (Marocchi, 2006; Marocchi et al., this issue); Kamchatka (Kepezhinskas et al., 1996; Arai et al., 2003; Ishimaru et al., 2006; Ishimaru and Arai, in press), Mariana fore arc (Ohara and Ishii, 1998).

(O'Reilly et al., 1991; Yaxley and Kamenetsky, 1999; Powell et al., 2004) (Table 1), whereas data for suprasubduction amphibole (S-Amph) are derived from Japan (Johnson et al., 1996; Abe et al., 1998), Kamchatka (Ishimaru et al., 2006; Ishimaru and Arai, in press) and Papua New Guinea (Gregoire et al., 2001) (Table 2). Trace element analyses of amphibole from Ichinomegata (Japan) were also carried out at the Arc National Centre of Geochemical Evolution and Metallogeny of Continents (GEMOC) (Table 3). To enlarge the suprasubduction amphibole (S-Amph) dataset, analyses from the Finero and Val d'Ultimo (Italian Alps) alpine peridotites, which are considered as examples of subduction-related metasomatism, are

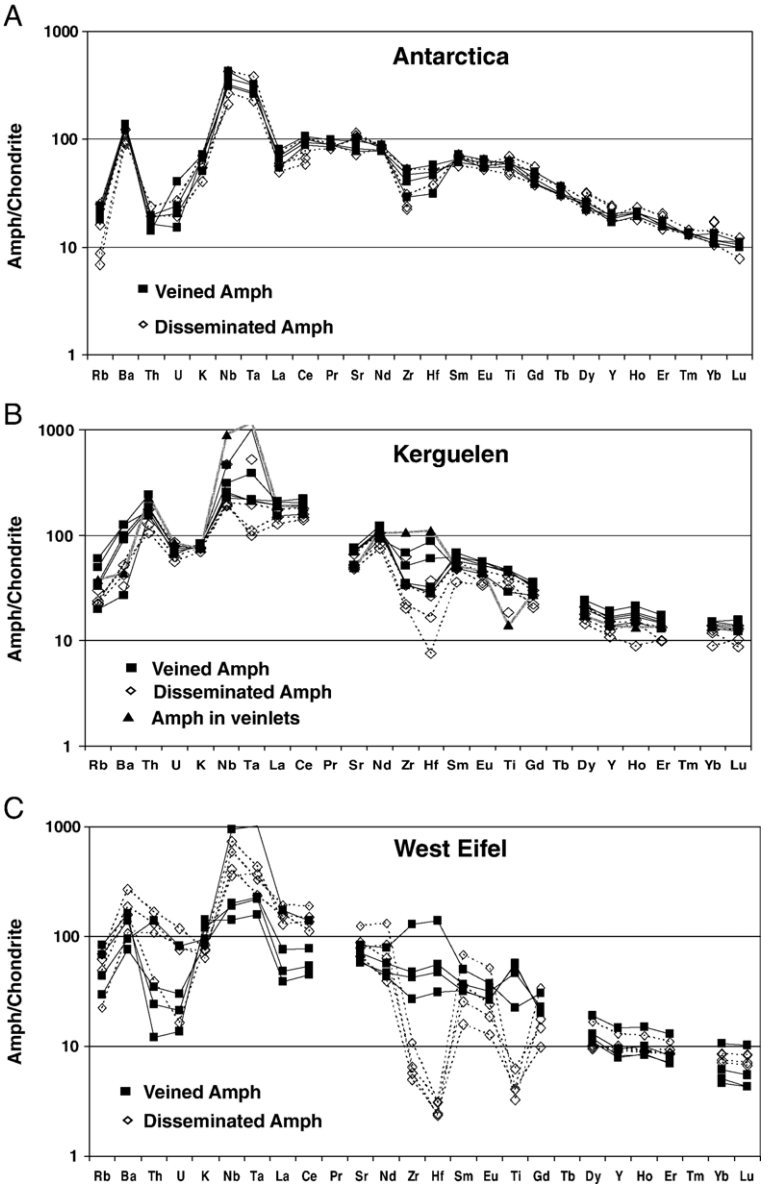

Fig. 2. Chondrite-normalized incompatible element diagrams for intraplate (A, B, C, D) and suprasubduction amphiboles (E, F). I-Amph data are from Antarctica (Coltorti et al., 2004), Kerguelen (Moine et al., 2001), West Eifel (Witt-Eickschen et al., 2003), Australia (O'Reilly et al., 1991; Yaxley and Kamenetsky, 1999: open diamond; Powell et al., 2004: black squares, Group A; black triangles, Group B; black diamonds, Group C; Coltorti unpublished data: open circles). S-Amph data are from Japan (Johnson et al., 1996; Abe et al., 1998; this work), Papua New Guinea (Gregoire et al., 2001), Kamchatka (Ishimaru et al., 2006; Ishimaru and Arai, in press), Val d'Ultimo (Marocchi, 2006; Marocchi et al., this issue), Finero (Zanetti et al., 1999). Normalizing values from McDonough and Sun (1995).

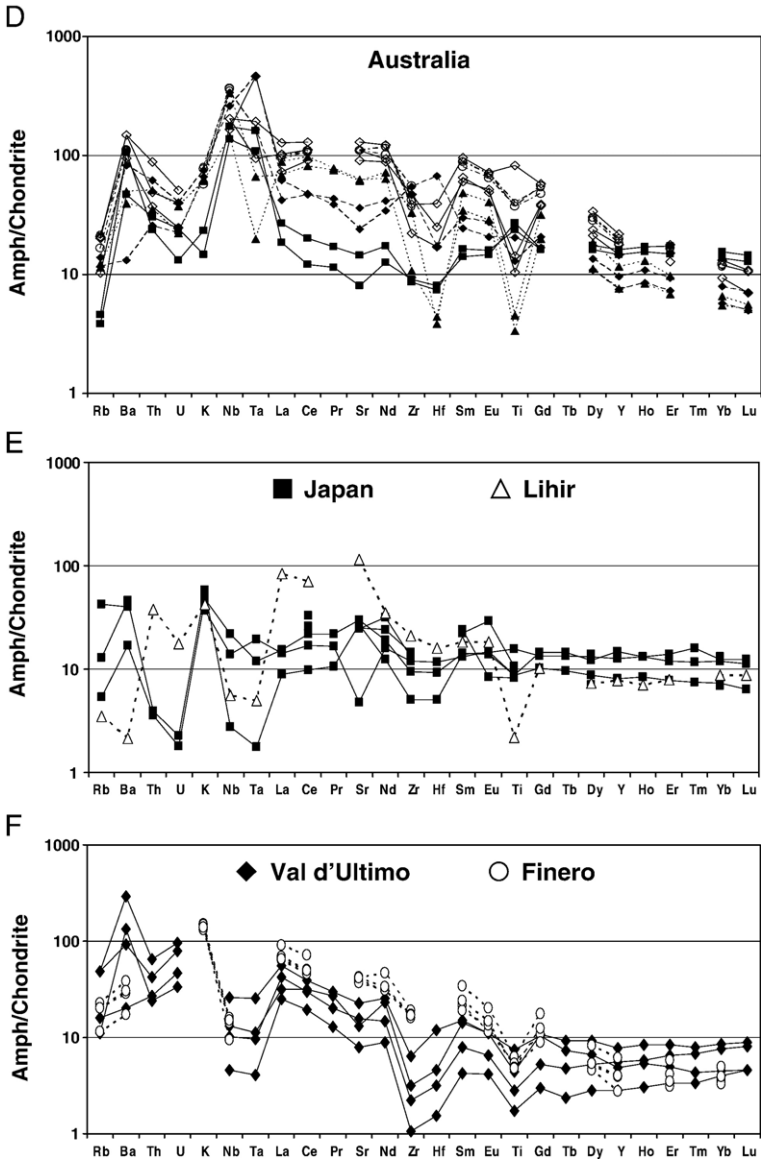

Fig. 2 (*continued*).

also included (Zanetti et al., 1999; Scambelluri et al., 2006; Marocchi, 2006; Marocchi et al., this issue).

3. Major and trace element data

Several studies have stressed the influence of SiO_2 and MgO contents in trace element partitioning behaviour in the amphibole (e.g. Tiepolo et al., 2000, 2001, 2003). The higher the degree of polymerization and the lower the mg# values of the melt, the higher the HFSE contents which should be expected to be incorporated within the amphibole. In order to separate crystallographic constraints from the pristine nature of the parental metasomatic agents, I-Amph and S-Amph with relatively restricted ranges of SiO_2 (40–48%) and mg# (80–94) were chosen (Fig. 1). Tiepolo et al. (2001) noted in fact that a great variation in $^{Amp/L}D_{Nb/Zr}$ occurs for amphibole with mg#<0.8. The variation in $^{Amp/L}D_{Nb/Zr}$ calculated in the present study according to Tiepolo et al. (2001) and with the above indicated mg# range is 0.43 ± 0.04, thus it can be assumed that this parameter does not affect the HFSE distribution. The same authors also noted that an increase in SiO_2 and a decrease in TiO_2 contents of the melts will increase the HFSE compatibility in amphibole (see also Marks et al., 2004). Beside the fact that metasomatic processes cannot

be directly equated to crystallization process, the two trends described are exactly opposite of those observed in amphibole from subduction and intraplate settings. It is well-known that suprasubduction environments are characterized by metasomatizing agents with higher degrees of SiO_2-saturation and lower TiO_2 contents with respect to their counterpart in intraplate settings, but S-Amph is characterized by the lowest Nb contents. As far as I-Amph is concerned no correlations between TiO_2 and Nb contents have been observed.

Based only on major elements, the dataset can be extended to amphiboles from the Pannonian Basin (Bali et al., 2002 and reference therein), Ahaggar (Dautria et al., 1987), Kamchatka (Kepezhinskas et al., 1996; Arai et al., 2003; Ishimaru et al., 2006; Ishimaru and Arai, in press) and Mariana (Ohara and Ishii, 1998). S-Amph generally shows lower Na_2O and TiO_2 contents than I-Amph, although a large overlap exists between the two groups (Fig. 1).

Chondrite-normalized incompatible trace element patterns of the selected amphiboles are shown in Fig. 2. Different patterns can be recognized within the intraplate amphibole group and, in some cases, these can be related to their microstructural occurrence. Xenoliths from Antarctica, Kerguelen and Eifel display both disseminated and vein amphiboles. In Antarctica both types have very similar geochemical features (Fig. 2A) (Coltorti et al., 2004), while at Kerguelen and Eifel they are geochemically distinctive (Fig. 2B, C) (Moine et al., 2001; Witt-Eickschen et al., 2003). Ti, Zr and Hf contents are highly variable: disseminated amphiboles commonly show Ti and Zr negative anomalies, while these are rare in veined amphibole. Amphiboles from western Victoria (Australia) are all disseminated and some are characterized by prominent Ti, Zr and Nb negative anomalies (Fig. 2D), which is interpreted as being due to carbonate-rich silicate or carbonatite metasomatism (Powell et al.,

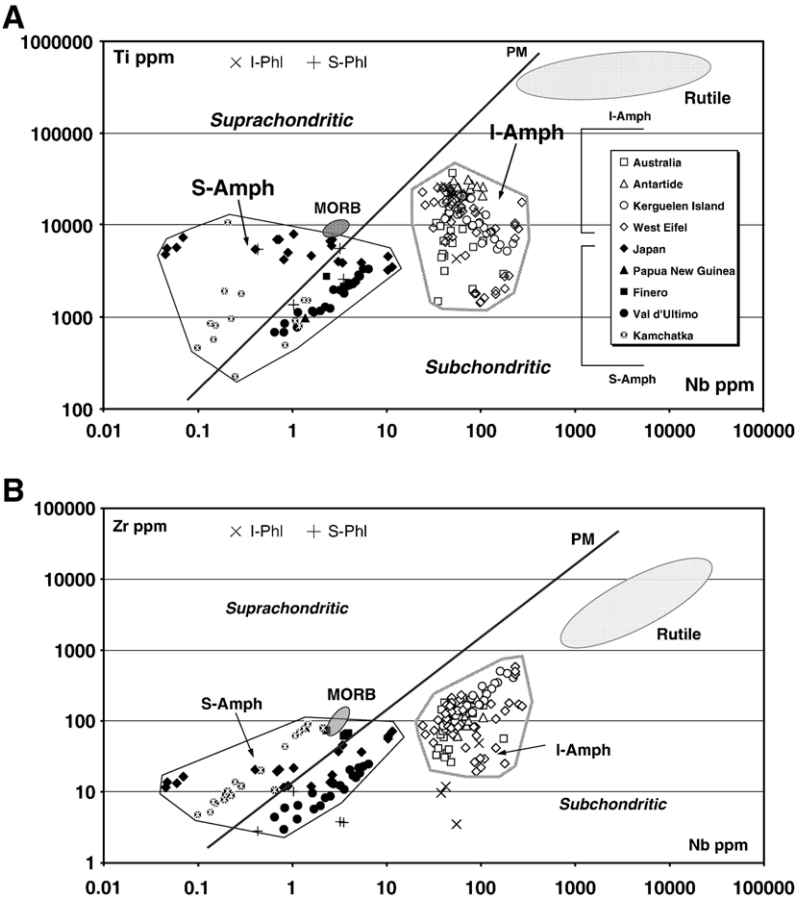

Fig. 3. Ti (A) and Zr (B) vs Nb diagrams for intraplate and suprasubduction amphiboles (data set as in Fig. 2). S-Amph, suprasubduction amphibole; S-Phl, suprasubduction phlogopite; I-Amph, intraplate amphibole; I-Phl, intraplate phlogopite. Rutile field is from Zack et al. (2002) and Kalfoun et al. (2002). MORB and Primordial Mantle (PM) values are from McDonough and Sun (1995).

2004), possibly related to an old subduction signature (Griffin et al., 1988). A few samples from East Eifel present quite low Nb contents due to the effect of subduction which affected this portion of the lithospheric mantle during Hercynian (Witt-Eickschen et al., 2003).

The observed compositional variation of these analyses (not included in the I-Amph group) is not the result of textural positions, but the effect of older metasomatic episodes. Textural position can affect HFSE distribution but the variation would be orders of magnitude lower than that introduced by tectonic imprinting (see also Coltorti et al., 2007).

On the other hand S-Amph, (mostly disseminated), shows a less enriched and fractionated pattern, with flat Heavy Rare Earth Elements (HREE) and well-pronounced Nb (and Ta where analyzed) negative anomalies (Fig. 2E, F).

I-Amph geochemical signatures are clearly discriminated from those for S-Amph by their higher Ba, Nb, Ta, Zr, Hf and Ti contents (Fig. 2). I-Amph also tends to have higher HREE contents and more fractionated HREE patterns than S-Amph.

When suprasubduction and intraplate metasomatic signatures are compared, phlogopite and clinopyroxene do not show geochemical characteristics as clearly as amphibole. Phlogopite is rarer than amphibole and, like clinopyroxene, does not incorporate the large spectrum of trace elements observed in amphibole. Nevertheless, phlogopites from the Kerguelen plateau (Moine et al., 2001) display higher Ba, Nb, Zr and Ti contents than phlogopites in xenoliths from Lihir (Papua New Guinea, Gregoire et al., 2001) and in exposed mantle peridotites from Finero (Northern Italy, Zanetti et al., 1999) (Fig. 3A, B). Intraplate clinopyroxenes tend to have higher Ti and Nb contents than orogenic clinopyroxenes although Ba and Nb concentrations are near detection limits and the data are quite scattered. Clinopyroxenes from Gran Comore, where carbonatitic metasomatism was recognized by Coltorti et al. (1999), have comparable Ti and Zr contents to those from Lihir,

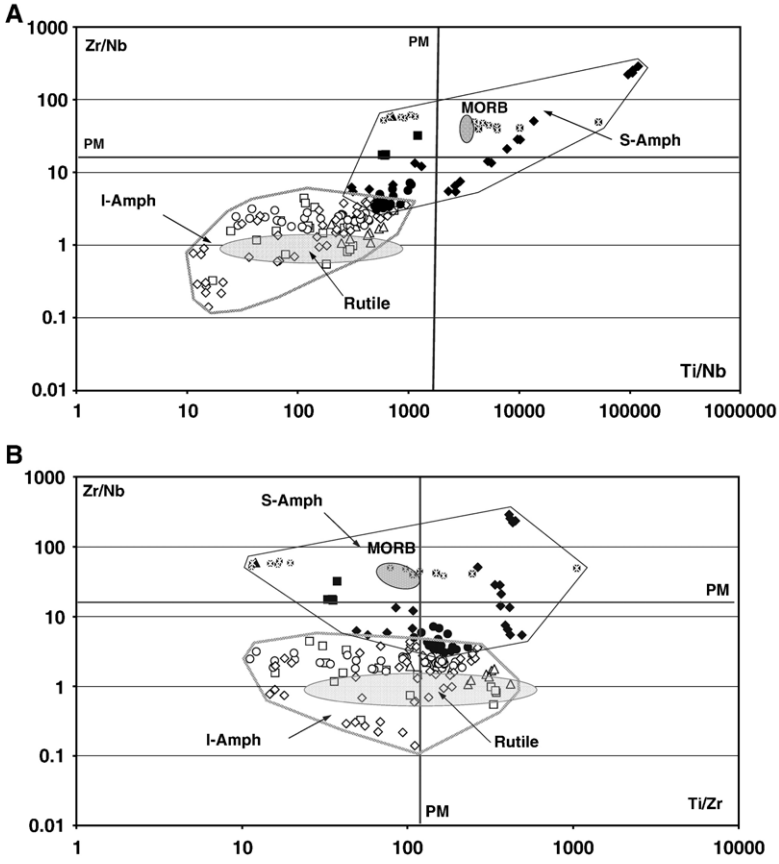

Fig. 4. Zr/Nb vs Ti/Nb (A) and Zr/Nb vs Ti/Zr (B) diagrams for intraplate and suprasubduction amphiboles. Data set, abbreviations and fields as in Fig. 2.

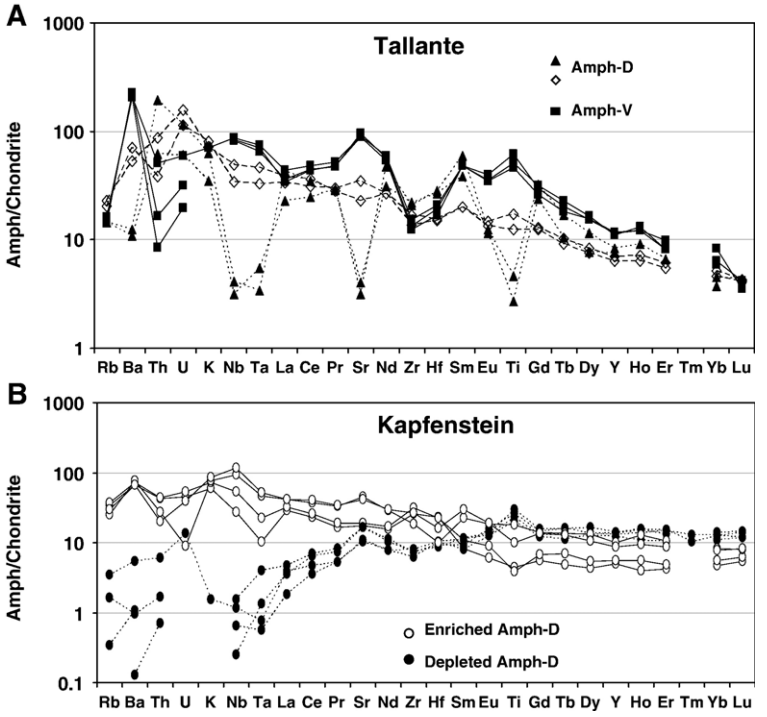

Fig. 5. Chondrite-normalized incompatible element diagrams for amphiboles from Tallante (Spain, this work and Coltorti unpublished data) and Kapfenstein (Austria, Coltorti et al., 2007). Amph-D, disseminated amphibole; Amph-V, amphibole in vein. Normalizing values from McDonough and Sun (1995).

but with much stronger negative anomalies reflecting higher REE concentrations.

In summary, suprasubduction amphiboles have consistently lower HFSE (and HREE) contents than I-Amph. In those cases where comparable Ti negative anomalies occur, intraplate minerals are distinguished by significantly higher Nb (and Ta when analyzed) contents. In addition, trace element analyses of phlogopites and clinopyroxenes from both intraplate and suprasubduction xenoliths indicate similar geochemical differences between the two tectonic settings.

4. HFSE distribution in orogenic and intraplate amphiboles

The ranges of Ti and Zr contents significantly overlap in amphiboles from both suprasubduction and intraplate settings (Fig. 3A and B). For single points

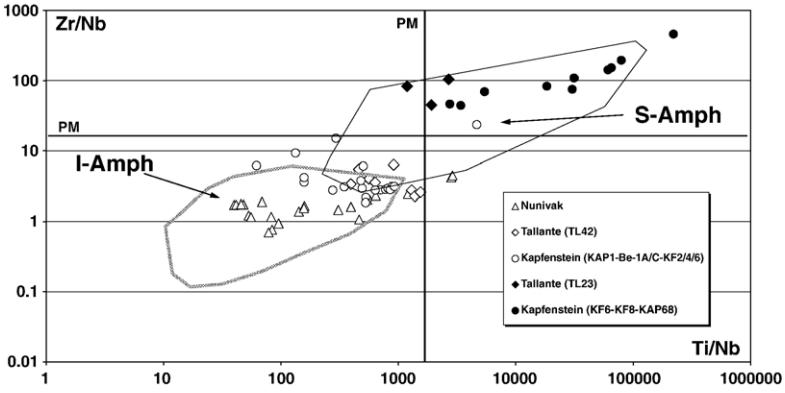

Fig. 6. Zr/Nb vs Ti/Nb diagram for amphiboles from Tallante (Spain, this work and Coltorti unpublished data), Kapfenstein (Austria, Coltorti et al., 2006; Faccini et al., 2006) and Nunivak (Alaska, this work). Abbreviations and fields as in Fig. 4.

however, there is a trend towards higher Ti, and to a lesser extent Zr, contents for I-Amph. However, S-Amph is always characterized by lower Nb contents for similar Zr and Ti values. Nb in particular represents the best element for discriminating between the two fields. It averages 75.7 ppm (±19.7) for the four I-Amph populations (Table 1), whereas it averages 2.54 ppm (+2.42) for the five S-Amph groups (Tables 2 and 3).

Notwithstanding the slight overlap, S-Amph has both Ti/Nb and Zr/Nb ratios straddling the chondritic values (Ti/Nb_{Ch} = 1823 (McDonough and Sun, 1995), $Ti/Nb_{S\text{-}Amph}$ = 118,774–306, average 6967; Zr/Nb_{Ch} = 15.7 (McDonough and Sun, 1995), $Zr/Nb_{S\text{-}Amph}$ = 290–3.07, average 39.4). In addition, the average for both ratios is suprachondritic for S-Amph. In contrast, I-Amph clearly shows subchondritic ratios for both Ti/Nb and Zr/Nb ($Ti/Nb_{I\text{-}Amph}$ = 948–11.3, average 266; $Zr/Nb_{I\text{-}Amph}$ = 4.43–0.14, average 2.07), due to the higher Nb content.

The distinctive geochemical signatures of S- and I-Amph can be well illustrated by plotting Zr/Nb ratios

Table 4
Representative analyses of S-Amph and I-Amph from Kapfenstein (Austria; Coltorti et al., 2007) and Tallante (Spain)

Locality	Kapfenstein						Tallante					
Amph-Type	I-Amph			S-Amph			I-Amph			S-Amph		
Sample	KAP1	KF2	KF4	KF2	KF6	KF6	TL42	TL42	TL42	TL23	TL23	TL23
Spot	9	C	B	B	E	G	6	7	8	1	2	3
SiO_2	42.58	43.38	43.22	43.10	42.74	42.60	40.81	40.99	42.36	43.29	43.06	43.24
TiO_2	3.89	0.98	0.65	1.18	2.04	2.15	5.02	3.79	3.46	0.78	0.34	0.20
Al_2O_3	14.08	14.69	15.28	15.46	15.57	15.58	13.96	13.90	13.24	14.14	13.89	14.82
FeO_{tot}	5.85	4.06	3.69	4.04	4.04	4.04	4.78	5.97	5.83	3.57	3.54	3.22
MnO	0.08	0.05	0.07	0.08	0.08	0.07	0.13	0.00	0.01	0.00	0.00	0.12
MgO	16.55	17.62	17.83	17.88	17.91	17.88	15.99	15.91	16.09	17.67	17.08	17.78
CaO	10.45	10.66	10.71	10.44	10.99	11.04	11.95	11.76	11.82	11.78	11.13	11.80
Na_2O	2.89	3.14	3.24	3.75	3.78	3.73	2.57	2.56	2.67	3.16	3.24	2.85
K_2O	1.24	1.27	1.30	0.63	0.02	0.02	1.04	1.19	1.19	0.49	0.50	0.92
NiO	0.03	0.09	0.06	0.11	0.12	0.12	0.08	0.09	0.06	0.14	0.14	0.16
Cr_2O_3	0.06	1.89	1.80	1.64	0.91	0.96	0.57	0.86	0.79	1.56	1.54	1.09
Total	97.70	97.82	97.84	98.31	98.20	98.19	96.91	97.02	97.52	96.59	94.46	96.20
mg#	83.43	88.55	89.59	88.73	88.76	88.74	85.63	82.60	83.10	89.81	89.58	90.78
Rb	9.14	10.4	13.8	4.22	1.23	2.11	5.64	5.47	4.93	16.0	5.03	5.01
Ba	251	203	181	106	13.0	18.9	507	497	547	47.0	26.1	29.8
Th	0.00	0.77	1.35	0.63	0.18	0.24	1.49	0.25	0.48	7.33	1.80	5.63
U	0.07	0.23	0.44	0.17	0.11	0.16	0.47	0.16	0.25	1.51	0.49	0.93
Nb	30.9	24.2	27.0	1.20	0.29	0.46	21.3	20.8	20.1	2.45	0.77	1.02
Ta	1.81	0.83	1.35	0.00	0.01	0.04	1.05	0.99	0.92	0.05	0.08	0.05
La	7.55	9.29	8.15	7.09	0.92	0.95	10.4	8.07	8.55	14.6	5.47	10.2
Ce	27.2	21.5	16.0	14.2	2.89	3.77	29.2	26.7	27.4	32.8	15.2	21.3
Pr	3.98	2.92	1.95	1.62	0.50	0.57	4.95	4.53	4.48	4.54	2.78	2.72
Sr	516	263	138	290	75.1	70.3	660	640	701	48.9	23.0	29.2
Nd	21.8	12.2	8.03	7.07	3.64	4.15	27.7	25.2	26.7	31.7	21.9	14.5
Zr	64.2	102	167	28.3	31.2	37.9	58.8	47.6	52.2	110	80	85
Hf	2.89	1.88	3.45	0.77	1.11	1.18	2.24	1.79	2.04	2.41	3.02	2.86
Sm	5.85	4.11	1.67	1.81	1.22	1.33	7.32	7.37	7.33	11.8	9.08	5.81
Eu	2.26	1.01	0.45	0.63	0.72	0.55	2.31	2.04	2.00	1.78	0.73	0.67
Gd	4.76	2.54	1.48	1.86	2.48	2.23	6.15	6.54	5.33	9.24	6.66	4.89
Tb	0.72	0.43	0.28	0.36	0.42	0.49	0.77	0.85	0.68	1.16	0.63	0.39
Dy	3.78	2.16	1.26	2.34	3.23	3.39	3.86	4.19	3.98	4.25	2.94	1.95
Y	14.4	12.5	9.15	14.1	19.2	18.3	18.1	17.5	18.3	20.6	13.1	11.8
Ho	0.81	0.45	0.30	0.51	0.61	0.75	0.69	0.75	0.68	n.d.	0.52	n.d.
Er	1.53	1.29	1.03	1.42	1.73	2.12	1.63	1.35	1.34	n.d.	1.09	n.d.
Tm	0.21	n.d.	n.d.	n.d.	n.d.	n.d.	n.d.	n.d.	n.d.	n.d.	n.d.	n.d.
Yb	1.30	1.32	0.96	1.33	1.83	2.02	1.41	1.09	1.00	n.d.	0.77	0.63
Lu	0.15	0.17	0.14	0.17	0.30	0.25	0.09	0.11	n.d.	n.d.	0.11	n.d.

mg# = [Mg/(Mg+Fe_t)*100]. n.d., not detected.

against Ti/Nb and Ti/Zr respectively (Fig. 4A and B). S-Amph is depleted in Nb as indicated by the suprachondritic values of Zr/Nb ratios, and this is almost perfectly counterbalanced by the subchondritic values of I-Amph, due to their Nb enrichment. Ti/Nb is also quite efficient in separating the two groups, although a small overlap is evident for Ti/Nb values around 1000. Ti/Zr ratios of the two groups of amphiboles are almost identical, thus, as also shown in the spidergram, the Ti/Zr ratio is not able to discriminate between orogenic and intraplate amphiboles.

5. Multiple metasomatic imprints

The proposed discrimination diagrams can be tested in those situations where multiple metasomatic episodes have been recognized. In this respect, two particularly interesting cases are represented by mantle xenoliths from Tallante (Southeastern Spain, Beccaluva et al., 2004; Shimizu et al., 2004) and Kapfenstein (Austria, Faccini et al., 2006; Coltorti et al., 2007;), where it is interpreted (based on textural and geochemical features), that an intraplate metasomatic event overprinted an older suprasubduction metasomatic episode.

Accordingly, two groups of amphiboles are clearly distinct in the Tallante xenoliths: Amphiboles from sample TL42 present more marked Ti than Nb positive anomalies, but they are always distinctly enriched in Nb, Ta and Ti relative to amphibole from sample TL23 (Fig. 5A, Table 4). This sample is in fact believed to still preserve the subduction signature (Beccaluva et al., 2004). In Fig. 6 amphiboles TL23 plot well within the orogenic field, while amphiboles TL42 tend towards the intraplate field.

Analogously two groups of amphiboles can be distinguished in Kapfenstein xenoliths (Table 4). Contrary to what was observed at Tallante, the two kinds of amphiboles (always disseminated) may even occur within the same sample (KF6, Fig. 6). In this case amphibole geochemical features straddle the I-Amph and S-Amph fields possibly recording a transition from suprasubduction to intraplate metasomatism (Figs. 5B and 6) (Coltorti et al., 2006; Faccini et al., 2006). Amphibole from the other samples are quite well discriminated by the diagram of Fig. 6. Depleted disseminated amphibole (Amph-D), which is believed to record a suprasubduction event, plots well within the suprasubduction field. Enriched Amph-D, which records successive intraplate metasomatic imprinting, tends towards lower Zr/Nb and Ti/Nb values and most of it falls into the intraplate field (Figs. 5B and 6).

Another well-known occurrence is the mantle xenoliths from Nunivak (Alaska, Francis, 1976; Roden et al., 1984). Xenoliths are brought to the surface by alkaline (s.l.) basalts and, notwithstanding the position of the island behind the Aleutian Arc, most of the analyzed amphiboles (Table 5) fall well within the I-Amph field suggesting a strong alkaline intraplate metasomatic activity.

From Fig. 6, it is noteworthy that amphiboles inferred to be derived from the two types of mantle tectonic domains reveal the same geochemical differences, and are clearly discriminated by the proposed diagrams.

6. The origin of HFSE and Nb depletion in S-Amph

It is well documented that Mid-Ocean Ridge Basalts (MORB) derive from a depleted mantle source, resulting in relatively low Nb content, and with suprachondritic ratios for both Zr/Nb and Ti/Nb. The field for MORB (McDonough and Sun, 1995) is shown on Figs. 3 and 4. In both diagrams the S-Amph field plots very close to, or encloses, the MORB field, emphasising the depleted character with respect to suprachondritic Zr/Nb and Ti/Nb.

The eclogite compositional field is more difficult to define and a more precise definition it is out of the scope of the present work. Eclogites in fact present a large compositional variation that includes the effects of the i) protolith composition, ii) element mobility during alteration, dehydration and transport to the Earth's surface (Chalot-Prat et al., 2003; Spandler et al., 2004), and iii) large modal variability. A way of approaching the question is to consider the analyses of single minerals constituting eclogitic rocks, namely clinopyroxene and rutile. According to distribution partitioning coefficients, Ti and Zr would be preferentially incorporated in clinopyroxene relative to Nb (GERM data set: http://earthref.org/GERM/main.htm), while pentavalent HFSE would be strongly fractionated in rutile (Foley et al., 2000; Schmidt et al., 2004). In Figs. 3 and 4 rutile analyses plot in the subchondritic side of the diagram for both Ti/Nb and Zr/Nb ratios, whereas clinopyroxenes (not reported in the diagrams) span both the suprachondritic and subchondritic side of the diagram (Kalfoun et al., 2002; Gregoire et al., 2002). The presence of rutile (or, to a lesser extent, ilmenite) however dominates the Nb and Ti budget of eclogitic rocks, as a few percent of this phase will result in a large increase of the budget of these elements (e.g. Zack et al., 2002; Kalfoun et al., 2002).

The very large eclogite field (not reported for sake of clarity in the diagrams) encloses those of MORB and S-Amph underlining the genetic relationship between these lithotypes. Accordingly the great majority of eclogites show suprachondritic Ti/Nb and Zr/Nb ratios, plotting in a intermediate position between those of eclogitic cpx and rutile (Rudnick et al., 2000; Barth et al., 2001; Zack et al., 2002).

Table 5
Major and trace element analyses of amphiboles from Nunivak Island (Alaska)

Sample	ASK12				66AHR63							ASK10							ASK5			
Spot	am1–1	am1–2	am5–1	am5–2	am1–1	am2–1	am3–1	am4–1	am5–1	am6–1	am7–1	am1–1	am1–2	am2–1	am3–1	am4–1	am5–1	am5–2	am1–1	am1–2	am2–1	am3–1
SiO_2	43.47	43.66	42.99	43.20	42.18	43.04	42.25	42.23	42.85	41.87	41.96	43.08	43.04	42.61	43.10	42.83	43.00	43.18	40.88	41.09	41.41	41.21
TiO_2	0.17	0.16	0.18	0.19	2.69	2.43	3.23	2.94	3.07	4.68	4.78	0.64	0.67	0.52	0.59	0.54	0.62	0.60	4.02	4.05	3.82	3.82
Al_2O_3	15.06	14.81	14.75	14.84	14.26	14.27	13.96	14.21	14.51	14.41	14.83	14.15	13.85	14.20	14.24	14.06	14.01	13.99	14.21	14.65	14.02	14.21
FeO_{tot}	4.13	4.01	4.22	4.18	4.48	4.48	4.75	4.59	4.75	5.21	5.21	4.17	4.11	4.13	4.12	4.05	4.20	4.13	7.81	7.71	6.29	6.68
MnO	0.04	0.08	0.07	0.06	0.04	0.05	0.08	0.06	0.05	0.08	0.08	0.07	0.06	0.03	0.05	0.05	0.03	0.07	0.12	0.10	0.03	0.05
MgO	18.36	18.30	18.23	18.18	16.48	17.01	16.74	16.90	16.96	16.31	15.83	17.92	17.73	17.71	17.74	17.69	17.92	17.89	14.51	14.49	15.11	14.90
CaO	10.15	10.09	10.06	10.18	10.02	10.40	9.99	9.94	10.15	10.31	10.52	10.86	10.90	10.91	10.77	10.93	10.91	10.82	9.92	9.95	9.91	9.86
Na_2O	3.89	3.79	3.93	3.88	3.45	3.17	3.72	3.39	3.40	3.61	3.60	3.14	3.07	3.13	3.09	3.06	3.16	3.16	3.24	3.22	3.15	3.22
K_2O	0.45	0.46	0.44	0.46	1.10	1.53	0.83	1.38	1.35	0.63	0.65	1.26	1.19	1.17	1.19	1.21	1.14	1.16	1.40	1.35	1.54	1.42
NiO	0.17	0.15	0.12	0.16	0.12	0.12	0.11	0.12	0.11	0.08	0.11	0.13	0.14	0.09	0.11	0.13	0.08	0.14	0.09	0.07	0.06	0.07
Cr_2O_3	0.97	1.05	1.22	1.15	1.41	0.47	1.20	0.33	0.19	0.12	0.08	1.34	1.31	1.84	1.29	1.31	1.34	1.31	0.28	0.28	0.63	0.91
Total	96.87	96.58	96.19	96.47	96.23	96.96	96.87	96.09	97.38	97.32	97.66	96.78	96.08	96.33	96.27	95.85	96.41	96.45	96.48	96.96	95.96	96.35
mg#	88.78	89.04	88.50	88.57	86.77	87.11	86.26	86.78	86.40	84.80	84.41	88.44	88.47	88.42	88.47	88.62	88.38	88.52	76.79	76.98	81.04	79.88
Rb	1.39	1.41	1.43	1.38	8.17	6.02	3.29	5.10	4.56	2.74	2.76	12.4	12.2	13.4	13.8	12.8	12.0	11.3	7.64	8.17	10.1	9.90
Ba	74.1	75.6	75.6	77.2	225	152	157	145	144	113	112	308	343	347	295	283	347	322	219	195	257	252
Th	0.37	0.43	0.38	0.40	0.39	0.40	0.39	0.39	0.41	0.07	0.08	1.74	1.72	1.77	1.68	1.78	1.86	1.76	0.65	0.66	0.75	0.81
U	0.31	0.32	0.30	0.33	0.10	0.12	0.13	0.09	0.11	0.08	0.06	0.58	0.53	0.54	0.55	0.50	0.48	0.48	0.19	0.19	0.23	0.25
Nb	25.2	25.0	24.7	24.6	29.9	97.4	15.8	110	117	9.67	9.38	39.1	69.4	42.7	62.4	46.2	42.1	44.5	35.3	41.5	71.0	55.8
Ta	1.67	1.66	1.68	1.79	0.74	6.19	0.28	5.18	6.17	0.40	0.42	2.19	2.85	2.37	2.64	2.22	2.49	2.46	1.76	1.81	3.51	2.67
La	5.66	5.91	5.65	5.65	9.79	12.7	9.15	11.3	11.2	1.86	1.92	22.0	24.4	25.1	24.3	23.3	24.2	23.4	10.1	10.7	12.3	12.1
Ce	27.5	27.7	27.5	27.2	21.0	30.0	20.2	33.4	31.4	6.98	6.94	41.9	54.9	52.1	56.0	47.0	46.5	44.8	28.0	30.0	35.0	33.2
Pr	5.61	5.59	5.59	5.55	2.81	4.75	2.95	5.90	5.47	1.55	1.55	3.75	6.69	5.45	6.61	4.92	4.94	4.86	4.35	4.65	5.20	4.96
Sr	780	859	785	825	434	429	507	454	461	493	500	881	848	900	870	842	874	868	669	645	650	647
Nd	27.7	27.7	28.1	27.9	11.6	23.3	13.1	30.4	27.8	9.92	10.1	9.53	24.9	16.4	24.1	14.8	14.9	15.4	21.5	22.2	23.9	23.5
Zr	43.5	43.5	43.1	43.6	32.1	135	38.9	184	183	40.7	41.9	37.0	84.8	50.0	72.5	88.0	32.3	31.2	82.0	85.0	104	90.7
Hf	2.86	2.82	2.79	2.80	0.55	5.06	0.90	6.17	6.66	1.42	1.45	0.41	1.02	0.51	0.94	0.77	0.38	0.37	2.35	2.45	2.98	2.46
Sm	5.90	5.77	5.83	5.98	2.56	5.50	3.23	7.86	7.05	3.77	3.89	1.35	4.44	2.15	4.08	1.95	1.92	2.27	6.12	6.13	5.90	5.95
Eu	1.84	1.86	1.86	1.84	0.95	1.64	1.25	2.26	2.12	1.59	1.62	0.68	1.47	0.92	1.34	0.87	0.85	0.87	2.25	2.18	2.12	2.17
Gd	3.94	3.86	3.88	3.93	2.66	5.32	3.13	6.41	6.22	4.28	4.60	1.66	3.62	2.14	3.32	1.98	2.06	2.26	6.20	5.78	5.44	5.71
Tb	0.47	0.46	0.49	0.48	0.39	0.72	0.52	0.88	0.83	0.68	0.72	0.35	0.57	0.39	0.50	0.36	0.40	0.40	0.92	0.87	0.83	0.84
Dy	2.37	2.43	2.51	2.45	2.32	3.89	2.82	4.72	4.64	3.73	3.74	2.74	3.52	3.06	3.26	2.70	2.98	3.00	5.26	5.25	4.86	5.06
Y	11.4	11.4	11.7	11.8	12.5	17.7	14.3	20.9	20.0	15.2	15.9	18.5	20.2	20.0	18.8	18.6	20.3	19.9	24.8	24.6	23.9	23.8
Ho	0.40	0.41	0.41	0.41	0.49	0.68	0.54	0.81	0.82	0.63	0.62	0.71	0.75	0.74	0.68	0.65	0.77	0.71	0.98	0.98	0.94	0.96
Er	0.95	1.02	1.01	1.00	1.16	1.58	1.37	1.89	1.86	1.29	1.38	1.98	2.06	2.14	1.91	1.86	2.23	2.07	2.41	2.29	2.30	2.29
Tm	0.13	0.14	0.14	0.14	0.17	0.20	0.17	0.23	0.21	0.15	0.15	0.34	0.29	0.32	0.26	0.29	0.31	0.30	0.32	0.31	0.30	0.29
Yb	0.87	0.90	0.89	0.92	1.00	1.27	1.11	1.39	1.31	0.84	0.88	1.97	1.87	2.04	1.81	1.89	2.10	1.99	1.74	1.73	1.85	1.78
Lu	0.13	0.13	0.13	0.13	0.15	0.17	0.18	0.18	0.17	0.11	0.12	0.31	0.27	0.30	0.26	0.27	0.31	0.31	0.25	0.25	0.25	0.24

For the analytical conditions see Powell et al. (2004) and the analytical methods section of the GEMOC website (http://www.es.mq.edu.au/gemoc/). mg#=[Mg/(Mg+Fe_t)*100].

In summary, S-Amph shares geochemical features similar to MORB, (Nb depletion and suprachondritic Zr/Nb and Ti/Nb ratios), with the field extending towards more depleted Nb values, in the opposite position to the rutile fields (Figs. 3, 4). If rutile (or ilmenite) was present in mantle xenoliths from orogenic settings, the distinctive Nb depletion in S-Amph may be easily explained by rutile preferentially retaining Nb with respect to Ti and Zr, as well as the overall HFSE depletion in S-Amph. This would in turn also explain the HFSE negative anomalies in calc-alkaline magmas. However there is no evidence for a large presence of rutile (or ilmenite) in orogenic mantle settings. Ayers et al. (1997) use experimental results to argue that rutile is not even stable in the mantle wedge above a subduction zone. As a consequence we have to consider that amphibole (as well as phlogopite and clinopyroxene) inherited its signature from the fluids extracted from the downgoing slab. This means that these fluids were originally relatively depleted in HFSE, with greater depletion in Nb than in Ti and Zr. During high pressure metamorphism rutile may form by reaction from ilmenite and/or titanite and, as testified by its wide presence in eclogites, it is a restitic product of slab melting or dehydration (Zack et al., 2002). This is a viable mechanism for generating HFSE-depleted fluids coming off the downgoing slab, and would result in the geochemical features observed in S-Amph. As evident in Fig. 4, rutile has exactly the complementary Zr/Nb and Ti/Nb ratios with respect to MORB, while having comparable Ti/Zr ratios. The eclogitic counterpart after MORB dehydration or melting will be thus enriched in HFSE and represent the best candidate for a Nb reservoir (Rudnick et al., 2000).

7. The origin of HFSE and Nb enrichment in I-Amph

The subchondritic Ti/Nb and Zr/Nb ratios in I-Amph must also be considered. The more incompatible behaviour of Nb with respect to Ti and Zr during mantle melting is not sufficient to explain the larger Nb enrichment observed in I-Amph, irrespective of their origin as products of metasomatic reaction (Coltorti et al., 2004) or as crystallization from a melt (Moine et al., 2001; Witt-Eickschen et al., 2003). Nor can the enrichment be attributed to different crystallochemical-structural arrangements, as the considered amphiboles share very similar major element compositions. Alkaline and highly alkaline basalts, from which I-Amph is considered to be ultimately derived, also tend to be enriched in Nb, leading to Ti/Nb and Zr/Nb subchondritic ratios.

The I-Amph field is located between primitive mantle (PM) and rutile compositions (Fig. 4A and B), with the eclogite field lying in between. Thus the role of rutile-bearing eclogite lenses in the genesis of Nb-rich alkaline basalts and eventually of I-Amph has to be taken into account. The link between a Nb-depleted component flushing the suprasubduction mantle wedge as recorded by S-Amph and a Nb-rich subducted component (eclogite) recorded ultimately in I-Amph is a feasible explanation. Rutile-bearing eclogite may be recycled as lenses and/or layers within the lower part of the upper mantle, providing a Nb-rich reservoir which will contribute to the genesis of alkaline magmas (McDonough, 1991; Fitton, 1995; Rudnick et al., 2000) and to the HFSE enrichment which has been observed in the deep lithosphere (Aulbach et al., 2004 and references therein). Silicate melt metasomatism could attain its HFSE budget by scavenging deep-seated rutile-bearing eclogitic lenses.

In this context it is also interesting to note that in several areas around the Mediterranean (Sardinia, Spain, Pannonian Basin, Serbia, Morocco, Algeria; Wilson and Downes, 2006 and reference therein) as well as in many subduction zones worldwide (New Zealand, Cook et al., 2005; Antarctic Peninsula, Hole, 1990; Patagonia, D'Orazio et al., 2001 and reference therein) alkaline volcanism commonly follows calc-alkaline (s.l.) magmatism on a timescale of a few to tens of millions of years. This evidence lends support to the link between subduction and generation of intraplate magmas. Physically the introduction of cold lithosphere could alone create instability within the upper mantle, but chemically a Nb-rich reservoir is necessary to take into account the enrichment of the alkaline magmas mantle source.

8. Conclusions

Our results demonstrate that Nb and Ti contents of amphiboles in mantle-derived peridotite xenoliths represent a robust new tool to constrain the tectonic nature of different mantle domains. Mantle amphiboles from intraplate domains have relatively high Nb within a rather restricted range of about 10–1000 ppm compared with those from suprasubduction domains, where Nb is generally below 10 ppm and with very little overlap. Thus the Ti/Nb ratios of mantle amphiboles provide an excellent discriminant for suprasubduction or intraplate tectonic environments and for the metasomatic episode that produced the amphibole. The S-Amph Ti/Nb and Zr/Nb ratios range from chondritic to slightly suprachondritic while those for I-Amph are subchondritic with very little overlap. Further discrimination is provided by the Zr/Nb ratio and plots of Zr/Nb against Ti/Nb and Zr/Nb against Ti/Zr. These discriminants are sufficiently sensitive to identify mantle domains that underwent multiple episodes of metasomatism related to different tectonic environments.

Metasomatic fluids coming off the subducting slab will be HFSE-depleted as a result of melting and/or dehydration of the oceanic crust and sediments, while HFSE-enriched fluids which infiltrate intraplate lithospheric mantle will be derived from Ti-rich-eclogites.

The model proposed by Ionov and Hoffman (1995) where two populations of Nb-rich and Nb-poor amphiboles should be present in the mantle wedge does not seem to be supported by the data reported in this work. All analyzed S-Amph appears in fact homogeneously depleted in Nb.

Acknowledgements

Norman Pearson is greatly acknowledged for providing invaluable support for the analytical work at Macquarie University. Suzy Elhlou is thanked for her kind assistance during in situ trace element analyses. Greg Yaxley and two anonymous referees are also thanked for their contribution to improve a previous version of the manuscript. The work benefited from fruitful discussions with Chris Hawkesworth. M. Coltorti, C Bonadiman and B. Faccini thank GEMOC for the use of the Geochemical Analysis Unit while they were visiting to undertake the analytical work for this project. This study was supported by an ARC Discovery Grant (SYO'R and WLG) and used instrumentation funded by ARC LIEF and DEST Systemic Infrastructure Grants, Macquarie University and Industry. This is contribution no. 471 from the ARC National Key Centre for the Geochemical Evolution and Metallogeny of Continents (www.es.mq.edu.au/GEMOC).

References

Abe, N., Arai, S., Yurimoto, H., 1998. Geochemical characteristics of the uppermost mantle beneath the Japan island arcs: implications for upper mantle evolution. Phys. Earth Planet. Inter. 107, 233–248.

Arai, S., Ishimaru, S., Okrugin, V.M., 2003. Metasomatized harzburgite xenoliths from Avacha volcano as fragments of mantle wedge of the Kamchatka arc: implication for the metasomatic agent. Isl. Arc 12, 233–246.

Aulbach, S., Griffin, W.L., O'Reilly, S.Y., McCandless, T.E., 2004. Genesis and evolution of the lithospheric mantle beneath the Buffalo Head Terrane, Alberta (Canada). Lithos 77, 413–451.

Ayers, J.C., Dittmer, S.K., Layne, G.D., 1997. Partitioning of elements between peridotite and H_2O at 2.0–3.0 GPa and 900–1100 degrees C, and application to models of subduction zone processes. Earth Planet. Sci. Lett. 150, 381–398.

Bali, E., Szabo, C., Vaselli, O., Torok, K., 2002. Significance of silicate melt pockets in upper mantle xenoliths from the Bakony–Balaton Highland Volcanic Field, Western Hungary. Lithos 61, 79–102.

Barth, M.G., Rudnick, R.L., Horn, I., McDonough, W.F., Spicuzza, M.J., Valley, J.W., Haggerty, S.E., 2001. Geochemistry of xenolithic eclogites from West Africa, part I: a link between low MgO eclogites and Archean Crust Formation. Geochim. Cosmochim. Acta 65, 1499–1527.

Beccaluva, L., Bianchini, G., Bonadiman, C., Siena, F., Vaccaro, C., 2004. Coexisting anorogenic and subduction-related metasomatism in mantle xenoliths from the Betic Cordillera (southern Spain). Lithos 75, 7567–7587.

Chalot-Prat, F., Ganne, J., Lombard, A., 2003. No significant element transfer from the oceanic plate to the mantle wedge during subduction and exhumation of the Thetys lithosphere (Western Alps). Lithos 69, 69–103.

Coltorti, M., Bonadiman, C., Hinton, R.W., Siena, F., Upton, B.G.J., 1999. Carbonatite metasomatism of the oceanic upper mantle: evidence from clinopyroxenes and glasses in ultramafic xenoliths of Grande Comore, Indian Ocean. J. Petrol. 40, 133–165.

Coltorti, M., Beccaluva, L., Bonadiman, C., Faccini, B., Ntaflos, T., Siena, F., 2004. Amphibole genesis via metasomatic reaction with clinopyroxene in mantle xenoliths from Victoria Land, Antarctica. Lithos 75, 115–139.

Coltorti, M., Bonadiman, C., Faccini, B., Ntaflos, T., Siena, F., 2007. Slab melt and intraplate metasomatism in Kapfenstein mantle xenoliths (Styria Basin, Austria. In: Coltorti, M., Downes, H., Piccardo, G.B. (Eds.), Melting, Metasomatism and Metamorphic Evolution in the Lithospheric Mantel. Lithos Special Issue, vol. 94, pp. 66–89.

Cook, R.C., Briggs, R.M., Smith, I.E.M., Maas, R., 2005. Petrology and geochemistry of intraplate basalts in the South Auckland Volcanic Field, New Zealand: evidence for two coeval magma suites from distinct sources. J. Petrol. 46, 473–503.

Dautria, J.M., Liotard, J.M., Cabanes, N., Girod, M., Briqueu, L., 1987. Amphibole-rich xenoliths and host alkali basalts. Petrogenetic constraints and implications on the recent evolution of the upper mantle beneath Ahaggar (Central Sahara, Southern Algeria). Contrib. Mineral. Petrol. 95, 133–144.

D'Orazio, M., Agostini, S., Innocenti, F., Haller, M.J., Manetti, P., Mazzarini, F., 2001. Slab window-related magmatism from southernmost South America: the late Miocene mafic volcanics from the Estancia Glencross Area (~52°S, Argentina–Chile). Lithos 57, 67–89.

Faccini, B., Bonadiman, C., Coltorti, M., Ntaflos, T., Siena, F., 2006. Subduction-related and intraplate metasomatism in Kapfenstein lithospheric mantle (Styrian Basin, eastern Austria). EGU 2006, Vienna 2–7 April 2006.

Fitton, J.G., 1995. Coupled molybdenum and niobium depletion in continental basalts. Earth Planet. Sci. Lett. 136, 715–721.

Foley, S.F., Barth, M.G., Jenner, G.A., 2000. Rutile/melt partition coefficients for trace elements and an assessment of the influence of rutile on the trace element characteristics of subduction zone magmas. Geochim. Cosmoch. Acta 64, 933–938.

Francis, D.M., 1976. Origin of amphibole in lherzolite xenoliths from Nunivak Island, Alaska. J. Petrol. 17, 357–378.

Gregoire, M., Lorand, J.P., O'Reilly, S.Y., Cottin, J.-Y., 2000. Armalcolite-bearing, Ti-rich metasomatic assemblage in harzburgitic xenoliths from the Kerguelen Islands: implications for the oceanic mantle budget of high-field strength elements. Geochim. Cosmochim. Acta 64, 673–694.

Gregoire, M., McInnes, B.I.A., O'Reilly, S.Y., 2001. Hydrous metasomatism of oceanic sub-arc mantle, Lihir, Papua New Guinea — part 2. Trace element characteristics of slab-derived fluids. Lithos 59, 91–108.

Gregoire, M., Bell, D.R., Le Roex, A.P., 2002. Trace element geochemistry of phlogopite-rich mafic mantle xenoliths: their

classification and their relationship to phlogopite-bearing peridotites and kimberlites revisited. Contrib. Mineral. Petrol. 142, 603–625.
Griffin, W.L., O'Reilly, S.Y., Stabel, A., 1988. Mantle metasomatism beneath western Victoria, Australia II: isotopic geochemistry of Cr-diopside lherzolites and Al-augite pyroxenites. Geochim. Cosmochim. Acta 52, 449–459.
Hole, M.J., 1990. Geochemical evolution of Pliocene—recent post-subduction alkalic basalts from Seal Nunataks, Antarctic Peninsula. J. Volcanol. Geotherm. Res. 40, 149–167.
Ionov, D., Hoffman, A.W., 1995. Nb–Ta-rich mantle amphiboles and micas: implications fro subduction-related metasomatic trace element fractionations. Earth Planet. Sci. Lett. 131, 341–356.
Ionov, D.A., O'Reilly, S.Y., Genshaft, Y.S., Kopylova, M.G., 1996. Carbonate-bearing mantle peridotite xenoliths from Spitsbergen: phase relationships, mineral compositions and trace element residence. Contrib. Mineral. Petrol. 125, 375–392.
Ionov, D.A., Griffin, L.W., O'Reilly, S.Y., 1997. Volatile-bearing minerals and lithophile trace elements in the upper mantle. Chem. Geol. 141, 153–184.
Ishimaru, S., Arai, S., in press. Calcic amphiboles in peridotite from Avacha volcano, Kamchatka, and their implications for metasomatic conditions in the mantle wedge. In: Coltorti, M. & Gregoire, M. Metasomatism in Oceanic and Continental Lithospheric Mantle, Geological Society of London Sp. Is.
Ishimaru, S., Arai, S., Ishida, Y., Shirasaka, M., Okrugin, M., 2006. Melting and multi-stage metasomatism in the mantle wedge beneath a frontal arc inferred from highly depleted peridotite xenoliths from the Avacha volcano, southern Kamchatka. J. Petrol. 48, 1–39.
Johnson, K.E., Davis, A.M., Bryndzia, L.T., 1996. Contrasting styles of hydrous metasomatism in the upper mantle: an ion microprobe investigation. Geochim. Cosmochim. Acta 60, 1367–1385.
Kalfoun, F., Ionov, D., Merlet, C., 2002. HFSE residence and Nb/Ta ratios in metasomatised, rutile-bearing mantle peridotites. Earth Planet. Sci. Lett. 199, 49–65.
Kepezhinskas, P., Defant, M.J., Drummond, M.S., 1996. Progressive enrichment of island arc mantle by melt-peridotite interaction inferred from Kamchatka xenoliths. Geochim. Cosmochim. Acta 60, 1217–1229.
Marocchi, M., 2006. Petrological and geochemical characterization of chlorite-peridotite from the Ulten Zone (Nonsberg-Ultental, Italy): implications on the metasomatic processes. PhD thesis, Bologna University.
Marocchi, M., Hermann, J., Morten, L., 2007. Evidence for multi-stage metasomatism of chlorite-amphibole peridotites (Ulten Zone, Italy): constraints from trace element compositions of hydrous phases. Lithos 99, 85–104 (this issue). doi:10.1016/j.lithos.2007.05.010.
Marks, M., Halama, R., Wenzel, T., Markl, G., 2004. Trace element variations in clinopyroxene and amphibole from alkaline to peralkaline syenites and granites: implications for mineral-melt and trace-element partitioning. Chem. Geol. 211, 185–215.
McDonough, W.F., 1991. Partial melting of subducted oceanic-crust and isolation of its residual eclogitic lithology. Philos. Trans.-R. Soc. Lond., Phys. Sci. Eng. 335, 407–418.
McDonough, W.F., Sun, S.S., 1995. The composition of Earth. Chem. Geol. 120, 223–253.
Menzies, M.A., Rogers, N., Tindle, A., Hawkesworth, C.J., 1987. Metasomatic and enrichment processes in lithospheric peridotites, an effect of asthenosphere–lithosphere interaction. In: Menzies, M.A., Hawkesworth, C.J. (Eds.), Mantle Metasomatism. London Academic Press Inc.
Moine, B.N., Gregoire, M., O'Reilly, S.Y., Sheppard, S.M.F., Cottin, J.-Y., 2001. High field strength element fractionation in the upper mantle: evidence from amphibole-rich composite mantle xenoliths from the Kerguelen Islands (Indian Ocean). J. Petrol. 42, 2145–2167.
Neumann, E.-R., Wulff-Pedersen, E., 1997. The origin of the highly silicic glass in the mantle xenoliths from the Canary Islands. J. Petrol. 38, 1513–1540.
Ohara, Y., Ishii, T., 1998. Peridotites from the southern Mariana forearc: heterogeneous fluid supply in mantle wedge. Isl. Arc 7, 541–558.
O'Reilly, S.Y., Griffin, W.L., 1996. 4-D lithosphere mapping; methodology and examples. Tectonophysics 262, 3–18.
O'Reilly, S.Y., Griffin, W.L., Ryan, C.G., 1991. Residence of trace elements in metasomatized spinel lherzolite xenoliths: a proton-microprobe study. Contrib. Miner. Petrol. 109, 98–113.
Powell, W., Zhang, M., O'Reilly, S.Y., Tiepolo, M., 2004. Mantle amphibole trace-element and isotopic signatures trace multiple metasomatic episodes in lithospheric mantle, western Victoria, Australia. Lithos 75, 141–171.
Roden, M.F., Frey, F.A., Francis, A.M., 1984. An example of consequent mantle metasomatism in peridotite inclusions from Nunivak Island, Alaska. J. Petrol. 25, 546–577.
Rudnick, R.L., Barth, M.G., Horn, I., McDonough, W.F., 2000. Rutile-bearing refractory eclogites: Missing link between continents and depleted mantle. Science 287, 278–281.
Scambelluri, M., Hermann, J., Morten, L., Rampone, E., 2006. Melt- versus fluid-induced metasomatism in spinel to garnet wedge peridotites (Ulten Zone, Eastern Italian Alps): clues from trace element, Li and Be abundances. Contrib. Mineral. Petrol. 151, 372–394.
Schmidt, M.W., Chazot, A.G., Vannucci, R., 2004. The dependence of Nb and Ta rutile-melt partitioning on melt composition and Nb/Ta fractionation during subduction processes. Earth Planet. Sci. Lett. 226, 415–432.
Shimizu, Y., Arai, S., Morishita, T., Yurimoto, H., Gervilla, F., 2004. Petrochemical characteristics of felsic veins in mantle xenoliths from Tallante (SE Spain): an insight into activity of silicic melt within the mantle wedge. Trans. Royal Soc. Edinburgh: Earth Sci. 95, 265–276.
Siena, F., Beccaluva, L., Coltorti, M., Marchesi, S., Morra, E., 1991. Ridge to hot-spot evolution of the Atlantic lithospheric mantle: evidence from Lanzarote peridotite xenoliths (Canary Islands). J. Petrol. 271–290 (Special Issue).
Spandler, C., Hermann, J., Arculus, R., Mavrogenes, J., 2004. Geochemical heterogeneity and element mobility in deeply subducted oceanic crust; insights from high-pressure mafic rocks from New Caledonia. Chem. Geol. 206, 21–42.
Szabo, C., Falus, G., Zajacz, Z., Kovacs, I., Bali, E., 2004. Composition and evolution of lithosphere beneath the Carpathian–Pannonian Region: a review. Tectonophysics 393, 119–137.
Tiepolo, M., Vannucci, R., Oberti, R., Foley, S., Bottazzi, P., Zanetti, A., 2000. Nb and Ta incorporation and fractionation in titanian pargasite and kaersutite: crystal-chemistry constraints and implications for natural systems. Earth Planet. Sc. Lett. 176, 185–201.
Tiepolo, M., Bottazzi, P., Foley, S., Oberti, R., Vannucci, R., Zanetti, A., 2001. Fractionation of Nb and Ta from Zr and Hf at mantle depths: the role of titanian pargasite and kaersutite. J. Petrol. 42, 221–232.
Tiepolo, M., Zanetti, A., Oberti, R., Brumm, R., Foley, S.F., Vannucci, R., 2003. Trace-element partitioning between synthetic potassic-richterites and silicate melts, and contrasts with the partitioning behaviour of pargasites and kaersutites. Eur. J. Mineral. 15, 329–340.

Wilson, M., Downes, H., 2006. Tertiary–Quaternary intra-plate magmatism in Europe and its relationship to mantle dynamics. In: Gee, D.G., Stephenson, R.A. (Eds.), European Lithosphere Dynamics. Memoirs, vol. 32. Geological Society, London, pp. 147–166.

Witt-Eickschen, G., Seck, H.A., Mezger, K., Eggins, S.M., Altherr, R., 2003. Lithospheric mantle evolution beneath the Eifel (Germany): constraints from Sr–Nd–Pb isotopes and trace element abundances in spinel peridotite and pyroxenite xenoliths. J. Petrol. 44, 1077–1095.

Yaxley, G.M., Kamenetsky, V., 1999. In situ origin for glass in mantle xenoliths from southeastern Australia: insights from trace element compositions of glasses and metasomatic phases. Earth Planet. Sci. Lett. 172, 97–109.

Zack, T., Kronz, A., Foley, S.F., Rivers, T., 2002. Trace element abundances in rutiles from eclogites and associated garnet mica schists. Chem. Geol. 184, 97–122 [26].

Zanetti, A., Mazzucchelli, M., Rivalenti, G., Vannucci, R., 1999. The Finero phlogopite–peridotite massif: an example of subduction-related metasomatism. Contrib. Mineral. Petrol. 134, 107–122.